Bibliographical reference

Positioning of Drops, Particles and Bubbles in Ultrasonic Standing-Waves Levitators. A Final Round Up, E. G. Lierke and L. Holitzner, Acta Acustica **vol. 99** (Number 2), 2013, pp. 302-316

DOI

https://doi.org/10.3813/AAA.918612

ACTA ACUSTICA UNITED WITH ACUSTICA
Vol. 99 (2013) 302 – 316

DOI 10.3813/AAA.918612

Positioning of Drops, Particles and Bubbles in Ultrasonic Standing-Waves Levitators. A Final Round Up

E. G. Lierke[1)], L. Holitzner[2)]

[1)] tec 5 AG, 61440 Oberursel, Germany. ernst-guenter@lierke.org

[2)] Laboratory for Developments and Methods, Paul Scherrer Institut, CH-5232 Villigen PSI, Switzerland. lothar.holitzner@psi.ch

Summary

This is a final round up of a series of articles, presentations and contract reports, which the author contributed to the pioneering of ultrasonic levitation in the European microgravity program between 1973 and 1995, followed by the redesign and promotion of the only commercial hardware concept for terrestrial applications, worldwide in use up to now. The article concentrates on rotational-symmetric, fluid filled Bessel-mode tube resonators. Theory and hardware concept of levitators for drops and particles in gases and for gas bubbles in liquids are quite similar but show specific differences. Special attention is given to design specifications, which allow the selection of optimal hardware and acoustic power range for experiments with drops and particles of defined size range in gases under different environmental conditions and for experiments with "small and large" gas bubbles in water. The Appendix offers brief guide lines for more detailed experiments with levitated bubbles. They explain characteristic cavitation phenomena, which are correlated with the ultrasonic degassing of oversaturated liquid/gas solutions and may help to understand the sudden death of whales near powerful military sonar systems.

PACS no. 43.35.-c

1. Introduction

Ultrasonic standing waves are three-dimensional variations of the sound pressure- and velocity amplitudes in a fluid medium as a result of multiple reflections between characteristic fluid/solid interfaces. Depending on the phase relation of the interfering components the sound field shows distinct minima (nodes) and maxima (antinodes) of the respective acoustic parameters. At typical frequencies between 20 and 100 kHz and wavelengths – in air between about 16 and 3 mm and in water between 7.5 and 0.5 cm – they are used to levitate drops, particles or bubbles with effective diameters up to about ½ of the wavelength λ at fixed positions without any mechanical contact ([1] through [7]). The effect is based on the fact, that the gravity force on samples with properties different from the fluid host medium, is compensated by a combination of acoustic *radiation pressure* (for the vertical support) and *Bernoulli under-pressure* (for the lateral stabilisation). Theory und design of ultrasonic-standing- wave levitators have initially been developed for microgravity experiments in US and European space programs. Later they were simplified for experiments on ground [2, 3] and optimized for specific samples (size, material, temperature, gas pressure) at different frequencies [8].

Figure 1a shows the cut view of a so called *open levitator* (tube diameter $> 12\lambda$) and in details 1b/c two water drops of 1 and 1,5 mm diameter, levitated in ambient air near neighbouring sound pressure nodes between the front face of a piezoelectric compound transducer [9] and a concentric, concave reflector at a resonance distance of about $5\lambda/2$. The stable drop positions enable an accurate long-term observation with the naked eye, a microscope or a video camera. Standard levitators [8] at 30, 58 and 100 kHz (section 3) allow physical/chemical experiments at gas/liquid or gas/solid interfaces at different environmental conditions with single drops or particles, having effective diameters between about 20 µm and 6 mm.

Received 18 January 2012,
accepted 23 September 2012.

2. Short description of the acoustic levitation concept

2.1. Basics of cylinder-symmetric positioning-force profiles

The positioning forces of a standing wave field result from the gradients of a multi-axial kinetic potential U, which is – according to equation (1) – the difference between potential energy density (*sound radiation pressure*) and kinetic energy density (*Bernoulli pressure*). The first is – according to equation (1b) – proportional to the square of

the sound pressure amplitude p, while the second – according to equation (1c) – is proportional to the square of the velocity amplitude v of the oscillating gas or liquid molecules. In general one finds for fluid media (liquids and gases) according to Barmatz and Collas [1]

$$U = E_{\text{pot}} f_1 - E_{\text{kin}} f_2, \tag{1a}$$

$$\text{with} \quad E_{\text{pot}} = \frac{p^2}{2\rho_0 c_0^2} \tag{1b}$$

$$\text{and} \quad E_{\text{kin}} = \frac{\rho_0}{2} v^2. \tag{1c}$$

The characteristic factors f_1 und f_2 in equation (1a) depend on the ratios of the densities ($\bar{\rho} = \rho_s/\rho_0$), sound velocities ($\bar{c} = c_s/c_0$) and the specific acoustic impedances ($\bar{Z} = \rho_s c_s/\rho_0 c_0$) of the respective partners, where the different parameters of the host medium (air or water) are marked with the index 0 and the sample parameters with the index s. This leads according to [1] to

$$f_1 = 1 - \frac{\rho_0 c_0^2}{\rho_s c_s^2} = 1 - \frac{\bar{\rho}}{\bar{Z}^2} \tag{2a}$$

$$\text{and} \quad f_2 = \frac{3(\rho_s - \rho_0)}{2\rho_s + \rho_0} = \frac{3(\bar{\rho} - 1)}{2\bar{\rho} + 1}. \tag{2b}$$

Longitudinal standing waves – with plane, horizontal wave fronts – are not suited for exact positioning, because they allow a free sample movement in lateral direction between the nodes or antinodes. Ideally suited are *open levitators* according to Figure 1 or *tube levitators* according to Figure 2 with radial gradients of the energy density, to provide radial stability. Both levitators are extensively described in the cited literature (e. g. [2] and [3]). The modular concept, shown in Figures 1a and 2, permits to switch from one to the other alternative by exchanging a few mechanical hardware components.

Standard, cylindrical *tube levitators* may be excited to plane longitudinal waves, with the sound velocity c_0 and to cylinder-symmetric wave modes [10], with node circles and radial gradients. These waves propagate with different axial sound velocity c_z and wave length λ and are – similar to the waves in the *open levitator* of Figure 1 – described by *Bessel*- or cylinder functions. The velocity potential

$$\Phi(z, r, t) = v_{\max}/k_0 \, J_0(k_r r) \cos(k_z z) \mathrm{e}^{\mathrm{j}\omega t} \tag{3}$$

between the front face of the ultrasonic transducer and the reflector or the tube bottom leads to

$$p(z, r) = \rho_0 \frac{\partial \Phi}{\partial t} = p_{\max} \, J_0(k_r r) \cos(k_z z) \tag{4}$$

for the sound pressure amplitude and

$$v_z(z, r) = -\frac{\partial \Phi}{\partial z} = v_{\max} \bar{k}_z \, J_0(k_r r) \sin(k_z z), \tag{5a}$$

$$v_r(z, r) = -\frac{\partial \Phi}{\partial r} = v_{\max} \bar{k}_z \, J_1(k_r r) \cos(k_z z) \tag{5b}$$

for the axial and radial velocity amplitudes respectively [1].

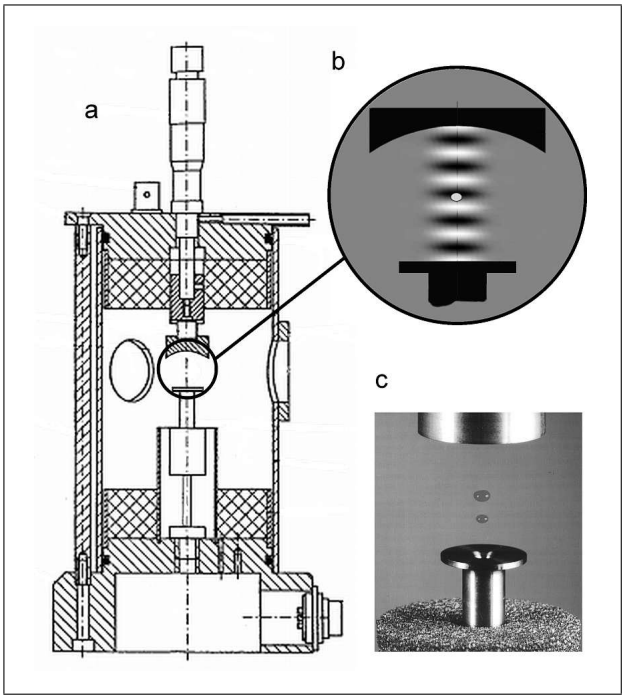

Figure 1. Gas-filled 58 kHz "open levitator" (a) with details (b) and (c) [3].

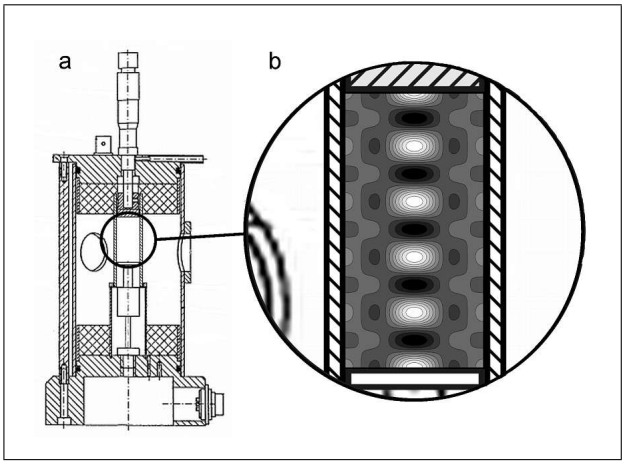

Figure 2. Gas-filled 58 kHz Bessel-mode tube levitator (a) with normalized potential distribution (8) as detail (b).

In the relevant range near the tube axis one can approximate the Bessel functions $J_0(k_r r) \approx \cos(k_r r/\sqrt{2})$ and $J_1(k_r r) \approx 0.5 \sin(k_r r)$. The solid reflector, at $z = 0$ and at the radiating transducer front face at $z = L$ coincide with nodes of the velocity amplitude and antinodes of the sound pressure amplitude.

The *dispersion-equation* for axial-radial wave propagation,

$$k_0^2 = k_r^2 + k_z^2 \quad (\text{normalized: } \bar{k}_z^2 + \bar{k}_r^2 = 1) \tag{6}$$

correlates the wave number $k_0 = \omega/c_0 = 2\pi/\lambda_0$ of the ideal longitudinal wave with the axial and radial wave numbers $k_z = \omega/c_z = 2\pi/\lambda_z$ and $k_r \approx \sqrt{2}\, 2\pi/\lambda_r$ of the Bessel mode, with the normalized values $\bar{k}_r = k_r/k_0$ and

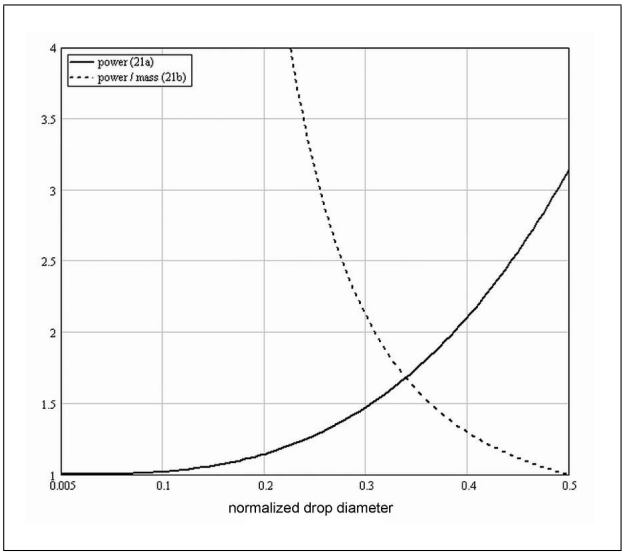

Figure 3. Normalized power (equation (21a) normalized with the value at $\bar{d}_s = 0$) and normalized power/mass-ratio (equation (21b) normalized with the value at $\bar{d}_s = 0.5$).

$\bar{k}_z = \sqrt{1 - \bar{k}_r^2}$. Both parameters follow from the radial boundary conditions (section 2.2).

The amplitudes $p_{\max}$ and $v_{\max}$ at the sound pressure and velocity antinodes are axially separated by $\lambda_z/4$ and coupled by the specific acoustic impedance Z_0 according to

$$p_{\max} = Z_0 v_{\max}, \tag{7}$$

with $Z_{0.a} = \rho_0 c_0 \approx 429\sqrt{T/T_=}$ [kg/m^{2}s] for air and $Z_{0,w} = 1.5 \cdot 10^6$ [kg/m^{2}s] for water.

This allows to replace the two energy densities

$$E_{\text{pot}}(p_{\max}) = E_{\text{kin}}(v_{\max}) = J/c_0$$

in equations (1b,c) by a single average sound intensity J. From equation (1) through (6) we find therefore a normalized equation for the kinetic potential

$$\begin{aligned}\bar{U}(r,z) &= U(r,z)/K^* \\ &= J_0^2(k_r r)\left[f_1 \cos^2(k_z z) - f_2 \bar{k}_z^2 \sin^2(k_z z)\right] \\ &\quad - f_2 \bar{k}_r^2 J_1^2(k_r r)\cos^2(k_z z).\end{aligned} \tag{8}$$

A normalization constant K^* (cf. equation 16) leads with (8) to the normalized axial levitation force

$$\begin{aligned}\bar{F}_z &= \frac{F(0,z)}{K^*} = -\frac{\partial \bar{U}(0,z)}{\partial z} \\ &= \left(f_1 + f_2 \bar{k}_z^2\right) k_z \sin\left(2k_z(z - z_0)\right)\end{aligned} \tag{9}$$

and – at $z_{0,1} = (2n+1)\lambda_z/4$ and $z_{0,2} = n\lambda_z/2$ respectively – to the different radial main forces

$$\begin{aligned}\bar{F}_{r,1} &= \frac{F(r,z_{0,1})}{K^*} = -\frac{\partial \bar{U}(r,z_{0,1})}{\partial r} \\ &\approx -\frac{2}{3} f_2 k_r \bar{k}_z^2 \sin\left(1.5 k_r r\right)\end{aligned} \tag{10a}$$

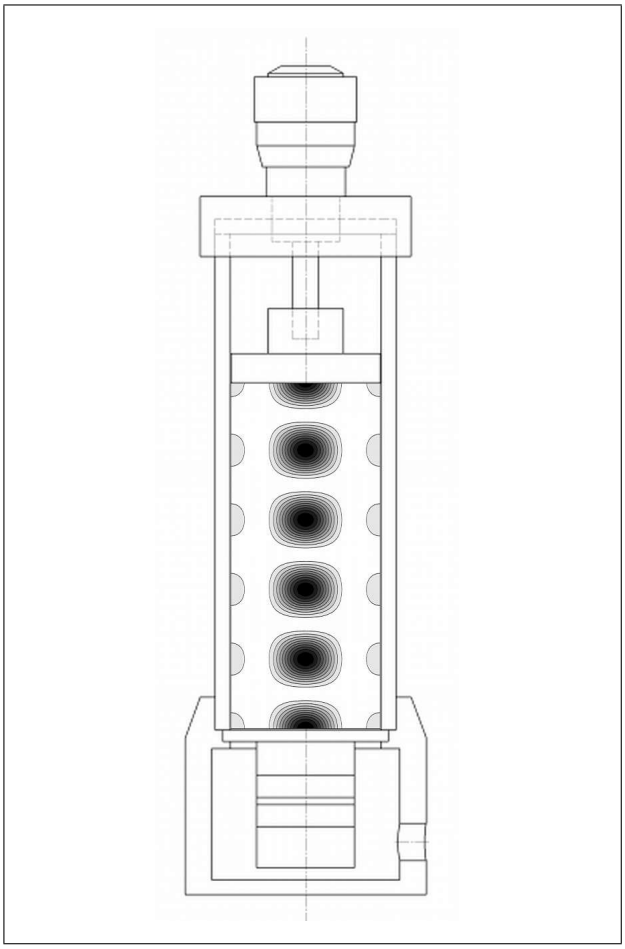

Figure 4. Water-filled Bessel-mode tube levitator with normalized radiation pressure profile for gas bubble levitation.

at the pressure nodes and

$$\begin{aligned}\bar{F}_{r,2} &= \frac{F(r,z_{0,2})}{K^*} = -\frac{\partial \bar{U}(r,z_{0,2})}{\partial r} \\ &\approx -\frac{2}{3} f_2 k_r \left(f_1/f_2 + 0.5\bar{k}_r^2\right) \sin\left(1.5 k_r r\right)\end{aligned} \tag{10b}$$

at the pressure antinodes.

Depending on the host medium and the characteristic factors f_1 und f_2, either the sound pressure nodes or antinodes become attraction centres ($\bar{U} < 0$) for small samples in their vicinity. Figure 2 shows periodic variations of the potential $\bar{U}$ in a gas levitator according to equation (8), represented by different grey levels, with repulsing zones (light) and attracting zones (dark). The isobars are more or less flat rotational ellipsoids with aspect ratios $a(r)/b(z)$ proportional to $1/\bar{k}_r$. The dark attraction centres coincide with pressure nodes and radial attraction forces according to equation (10a). These attraction zones at the pressure nodes disappear completely for gas bubbles in liquid filled levitators with $|f_1| \gg f_2 = 3$ (cf. Figure 4 and section 4). In this case "small" bubbles (with diameters below resonance and $\bar{U} < 0$) are attracted by the dominant radiation pressure at the sound pressure antinodes with radial forces according to equation (10b), while "large" bubbles (with

diameters above resonance and $\bar{U} > 0$) are repulsed in all directions.

2.2. The wave number ratio as key design parameter

The key design parameter of a tube levitator is the normalized wave number $\bar{k}_r < 1$. With the radial and axial boundary conditions it also defines the length/diameter ratio of the levitator tube. The axial velocity nodes at the two solid, totally reflecting tube ends ($z = 0$ and $z = L$) lead with $n = 1; 2; 3$ etc. to the tube length $L = n\lambda_z/2 = n/2\lambda_0/\sqrt{1-\bar{k}_r^2}$, while the radial velocity nodes at the tube wall ($k_r r = k_r\, D/2 = 3.832$) lead to the tube diameter $D = 1.22\lambda_0/\bar{k}_r$. This results in

$$\frac{L}{D} = \frac{n}{2.44}\frac{\bar{k}_r}{\sqrt{1-\bar{k}_r^2}} = \frac{n}{2.44}\frac{\sqrt{1-\bar{k}_z^2}}{\bar{k}_z} \tag{11}$$

shown as example in Figure 2b with $\bar{k}_r = 0.75$ and $n = 5$. The axial/radial wave propagation is associated with an increase of the axial tube wave-length λ_z relative to λ_0 of the plane longitudinal wave, described by

$$\frac{\lambda_z}{\lambda_0} = \frac{k_0}{k_z} = 1/\sqrt{1-(1.22c_0/fD)^2} = \sqrt{1+(1.22c_z/fD)^2}. \tag{12}$$

The so called 0/1-*Bessel-mode-wave* [10] – with 0 node diameters and 1 node circle – disappears at the *cut-off-wavelength* $\lambda_0 = D/1.22$. Cylindrical tubes with diameters $D \le 1.22\lambda_0$ carry therefore only plane waves *without* the required radial gradients. None-desirable interferences of the two wave modes may be suppressed, by tuning the tube length to resonance for the 0/1-Bessel-mode and to anti-resonance for the plane wave (cf. [2] and section 3.4).

2.3. Main forces and axial/radial force ratio

If the levitator axis is vertically aligned, the radial forces (10a,b) of terrestrial levitators are of second order priority. Sufficient approximations for the normalized axial force and the radial/axial force ratio,

$$\frac{F_{r,\max}(z_{0,1})}{F_{z,\max}} \approx \frac{2}{3}\frac{\bar{k}_r\sqrt{1-\bar{k}_r^2}}{1+f_1/f_2-\bar{k}_r} \tag{13a}$$

and

$$\frac{F_{r,\max}(z_{0,2})}{F_{z,\max}} \approx \frac{2}{3}\bar{k}_r\frac{f_1/f_2+0.5\bar{k}_r^2}{1+f_1/f_2-\bar{k}_r^2} \tag{13b}$$

follow from the maxima of equations (9) and (10a,b).

The essential vertical axial-force F_z according to equation (9) depends on the effective sample size and the distance $\Delta z = z - z_0$ between sample centre and pressure node or antinode respectively. In this position the axial force compensates the effective sample weight $V_s(\rho_s - \rho_0)g_0$ or buoyancy (cf. right side of equation 17) in a stable equilibrium. The integration of the 3-dimensional force profile across the idealized spherical sample surface (cf. [3]) leads together with the effective sample volume V_s and the abbreviations

$$\Phi_s = 1/\sin(2\pi\Delta z/\lambda_z) > 1, \tag{14}$$

called *levitation safety factor*,

$$f_s(\bar{d}_s) \approx 1 + 17.1\left(\bar{d}\right)^3 \le \pi \quad (\bar{d}_s = d_s/\lambda_z \le 0.5) \tag{15}$$

for the *sample size factor* [2] and

$$K^* = J/2c_0V_s/f_s(\bar{d}_s) \tag{16}$$

for the normalization factor of equation (8) to the axial levitation force

$$F_z(z,0) = \frac{J}{2c_0}\frac{V_s/\Phi_s}{f_s(\bar{d}_s)}\left(f_1+\bar{k}_z^2 f_2\right)k_z = \left(\rho_s-\rho_0\right)V_s g_0. \tag{17}$$

2.4. Required sound intensity and sound pressure amplitude

The required sound intensity (18) for safe axial levitation with $\Phi_s > 1$ follows from equations (14) through (17) (cf. [3] and [4]):

$$J(\rho_s,\bar{k}_z,\bar{d}_s,f) \approx \frac{1}{\pi}\left(\rho_s-\rho_0\right)\left[1+17.1(\bar{d}_s)^3\right]\frac{\Phi_s g_0 c_0\lambda_z}{f_1+f_2\bar{k}_z^2} \ge 1.55\frac{\Phi_s g_0 c_0 d_s}{f_1+f_2\bar{k}_z^2}\left(\rho_s-\rho_0\right) = J_{\min}(d_s). \tag{18}$$

The minimum at the right side of equation (18) allows a frequency optimization for a selected sample diameter $d_s \approx \lambda_z/\pi$. The respective sound pressure and velocity amplitudes follow with (7) from

$$\frac{p_{\max}/\sqrt{2}}{N/m^2} \approx \sqrt{Z_0\frac{J(\rho_s,\bar{k}_z,\bar{d}_s,f)}{W/m^2}} = Z_0\frac{v_{\max}/\sqrt{2}}{m/s}. \tag{19}$$

At a typical levitation safety factor $\Phi_s = \sqrt{2}$ the effective sample centre is stably positioned at a distance $\lambda_z/16$ below the selected pressure node. At a safety factor $\Phi_s < 1$ ($\Delta z > \lambda_z/8$) the sample will be dropped and with growing $\Phi_s > 1$ it approaches the pressure node asymptotically from below.

2.5. Acoustic power requirement

The required acoustic power P for samples, levitated at known sound intensity $J(k_z d_s)$ in a tube levitator of diameter $D = 2R$ can be estimated from the integral of the Bessel-function $J_0^2(k_r r)$ (8) across the full cross section of the levitator tube. Considering the factor

$$2\pi\int_0^R J_0^2(k_r r)\, r\,\mathrm{d}r = \frac{2\pi}{k_r^2}\int_0^{3.83} J_0^2(x)\, x\,\mathrm{d}x \approx \frac{7.5}{k_r^2} \tag{20}$$

and the effective sample mass $m_s = (\rho_s - \rho_0)\pi/6d_s^3$ equation (18) leads to

$$P(\rho_s, \bar{k}_z, \bar{d}_s, f) \approx 0.06(\rho_s - \rho_0)\frac{\bar{k}_z^2/\bar{k}_r^2}{f_1 + f_2\bar{k}_z^2}\Phi_s \cdot g_0 c_0 \lambda_z^3\left[1 + 17.1\bar{d}_s^3\right] \leq P_{\max}(d_{s,\max}), \quad (21a)$$

with

$$\frac{P}{m_s} \approx 2.9\frac{\bar{k}_z^2/\bar{k}_r^2}{f_1 + f_2\bar{k}_z^2}\frac{1 + 17.1\bar{d}_s^3}{25.1\bar{d}_s^3}\Phi_s g_0 c_0 \geq 2.9\frac{\bar{k}_z^2/\bar{k}_r^2}{f_1 + f_2\bar{k}_z^2}\Phi_s g_0 c_0 \quad (\bar{d}_s < 0.5). \quad (21b)$$

The required acoustic power varies between $P_{\min}$ at $d_s \ll \lambda_z$ and $P_{\max} = \pi P_{\min}$ at $d_{s,\max} = \lambda_z/2$.

The ratio of acoustic power and sample mass reaches its minimum (right side of equation 21b) at the critical value $d_{s,\max} = \lambda_z/2$. Equations (21a,b) are therefore suitable to estimate the required dynamic power range of a levitator at given maximum sample size $d_s = \lambda_z/2$ and sample mass m_s. Since this theoretical maximum for spherical samples has never been reported, we recommended, to limit the sample diameter to the optimal value $d_{s,\text{opt}} \approx \lambda_z/\pi$

3. Levitation of drops and particles in gases ($f_1 = 1$ und $f_2 = 1.5$)

3.1. Design alternatives

Open levitators according to Figure 1a incorporate a removable, protective glass tube, more than ten wavelengths in diameter with several feed-throughs. They provide easy access for observation, sample deployment, manipulation and extraction and are used at frequencies up to 100 kHz. These levitators tolerate none-isothermal heating conditions with laser or gas blast. Tube levitators have an additional resonance tube according to Figure 2 and are better suited, if well defined and variable environmental conditions around the sample (temperature, static pressure, humidity etc.) are required. Because of too small tube dimensions at $f > 60$ kHz (cf. Table I) they are better suited for low ultrasonic frequencies. Both levitators are resonance tuned by axial movement of the reflector (tube bottom) with a micrometer screw under feed back control from the output voltage of the power supply. A more sophisticated, automatic resonance tuning with a stepper motor under phase-locked-loop feed back from a piezoelectric sensor at the reflector front-face (pressure antinode) is possible [2].

3.2. Special design features of the open levitator

Open levitators according to Figure 1 have no effective radial boundary, because the shown tube walls are too far away. In this case the diameters D_{tr} and D_r of transducer front face and reflector, with their different directivity characteristics $[2J_1(x)/x]$ at $x = k_0 D/2 \sin\varphi$ determine the radial wave propagation and the effective parameter $\bar{k}_r$. During the experimental optimization of 20 kHz flight hardware for the microgravity program of the European Space Agency ESA [2] we found optimal conditions at a resonance distance $L = L_0 + \Delta L$ with the radius r_K of curvature of the concave reflector (cf. Figure 1b) according to

$$L = 2.5\lambda_0 \approx r_k \approx 0.8 D_r \approx 1.2 D_{tr} \quad \text{and} \quad L = 2.5\lambda_z = L_0/\bar{k}_z. \quad (22)$$

This leads in ambient air with $\bar{k}_z = 0.88$ (see below) to $L \approx 3.25$ cm at 30 kHz and $L \approx 1.68$ cm at 58 kHz.

In this case the concave reflector with its opening angle $\varphi_0 \approx \pi/5$ receives and returns the full *main lobe* of the radiation characteristics of the transducer. The preferred central pressure node about matches the effective *near-field-length* $N = (D_{1/2}^2 - \lambda_0^2)/4\lambda_0 \approx 5\lambda_z/4$ of transducer and reflector, which leads to smallest beam diameter and optimal power concentration. Axial and radial levitation-force measurements [2] and later executed, precise wavelength measurements –$\lambda_0 = 5.96$ mm, $\lambda_z = 6.72$ mm– with standard 58 kHz levitator in dry nitrogen at 21.2 °C [22] revealed $\bar{k}_r = 0.46$. The above conditions (22) guaranteed a resonance amplification of the sound pressure amplitude by a factor 15 to 20 as compared with the free-field radiation at the same transducer amplitude.

3.3. Special design features of the tube levitator

In the relevant parameter range $0 \leq \bar{k}_r \leq 0.75$ we find from (9) and (13a) with a tolerable inaccuracy < ±2% the approximations

$$\frac{F_{z,\max}(\bar{k}_r)}{F_{z,\max}(0)} \approx 1 - \bar{k}_r^2 \quad (23a)$$

and

$$\frac{F_{r,\max}(\bar{k}_r)}{F_{z,\max}(0)} \approx \frac{2}{3}\frac{\bar{k}_r\sqrt{1 - \bar{k}_r^2}}{5/3 - \bar{k}_r^2} \approx 0.4\bar{k}_r \leq 0.3. \quad (23b)$$

Table I shows an overview of the normalized values of axial wave length, tube diameter and tube length together with the number n of axial half-wavelengths (for a typical length/diameter ratio $L/D \approx 2$) as functions of the design parameter $\bar{k}_r$. Also shown are the relative axial (23a) and radial (23b) levitation forces. Typical values for D and L at 60 kHz are given in the last two lines. They can be transformed proportional to $1/f$, if other frequencies are to be used.

We recognize a linear increase of the radial/axial force ratio with increasing $\bar{k}_r \leq 0.75$, combined with a decrease of the tube dimensions L and D proportional to $1/\bar{k}_r$ and a decrease of the axial force proportional to $1 - \bar{k}_r^2$. The optimal design is a compromise with sufficient force ratio at a given frequency.

Table I. Characteristic parameter values in air filled tube levitators with $L/D \approx 2/1$ (* cf. Table II).

$\bar{k}_r$	0.25	0.30	0.35	0.40	0.45	0.50	0.54*	0.60	0.70	0.75
λ_z/λ_0	1.033	1.048	1.068	1.091	1.12	1.155	**1.19**	1.25	1.41	1.5
L/λ_0	9.8	7.9	6.5	6.9	5.6	5.2	**4.75**	4.4	4.2	3.75
D/λ_0	4.88	4.07	3.49	3.05	2.71	2.44	**2.26**	2.03	1.74	1.64
n	19	15	13	12	10	9	**8**	7	5	5
$F_{z,\max}(\bar{k}_r)/F_{z,\max}(0)$	0.93	0.91	0.88	0.84	0.80	0.75	**0.71**	0.63	0.50	0.44
$F_{r,\max}/F_{z,\max}$	0.10	0.12	0.14	0.16	0.18	0.20	**0.22**	0.25	0.28	0.30
D(60kHz)/cm	2.80	2.30	2.00	1.73	1.53	1.38	**1.29**	1.16	1.00	0.94
L(60kHz)/cm	5.56	4.6	3.9	3.7	3.2	2.95	**2.71**	2.48	2.24	2.10

3.4. Suppression of undesired double resonances in tube levitators at variable temperature

The interference of plane waves (λ_0) with the desired Bessel-mode (λ_z) may be a problem, if the isothermal gas temperature of the levitator is changed by a relative margin $\pm\Delta T/T_0$ around the average temperature T_0. In order to select a dominant $n\lambda_z/2$ tube resonance of the Bessel-mode, one can suppress a possible disturbing interference by anti-resonance tuning $(2m+1)\lambda_0/4$ of the longitudinal mode according to (24), for instance with

$$L = 2n\frac{\lambda_z(T_0)}{4} = (2m+1)\frac{\lambda_0(T_0)}{4} \tag{24}$$

at $n = 5, 6, 7, 8, \ldots$ and $m = n+1$.

This leads with (12) to

$$\bar{k}_r(T_0) = \sqrt{1-(1+3/2n)^{-2}} \tag{25}$$

and

$$L/D \approx 0.2\sqrt{(2n+3)^2-(2n)^2} \approx 0.6\sqrt{1+4n/3}. \tag{26}$$

The plane wave varies proportional to $\sqrt{T/T_0}$ while the Bessel-mode wave varies according to (12) proportional to $1/\sqrt{1-k_r a2(T_0)T/T_0}$. If the tube length L is automatically adjusted, in order to keep the Bessel-mode in $n\lambda_z/2$ resonance during heat up and cool down, this would lead to common resonances with plane waves at

$$L(T_{\min,\mathrm{crit}}) = \frac{n+1}{2}\lambda_0(T_{\min,\mathrm{crit}})$$
$$\text{and}\quad L(T_{\max,\mathrm{crit}}) = \frac{n+2}{2}\lambda_0(T_{\max,\mathrm{crit}}). \tag{27}$$

Double resonances according to (27) require

$$\frac{T_{\mathrm{crit}}}{T_0} = 1 \pm \frac{\Delta T_{\mathrm{crit}}}{T_0} = \frac{1-[1+(3\pm1)/2n]^{-2}}{1-[1+3/2n]^{-2}} \tag{28}$$

(cf. Table II) and would lead to intolerable deformations of the potential profile of Figure 2b. If we consider however the typical, measured halve-value-width $\Delta T_{-3\mathrm{dB}}/T_0 \approx 2\%$ of the resonance curve of tube levitators versus temperature at constant frequency [11] and avoid a small, about $\pm 5\%$ range near $T_{\min,\mathrm{crit}}$ and $T_{\max,\mathrm{crit}}$, we find under the above conditions ($5 \le n \le 8$) with

$$0.5 \le \frac{T_{\max}-T_{\min}}{T_{\min}} \le 0.6. \tag{29}$$

Table II. Conditions for the resonance excitation of the 0/1-Bessel-mode combined with an anti-resonance suppression of the 0/0-longitudinal wave in a tube levitator according to (24) through (28). Preferred gas levitators at 30 kHz and 58 kHz.

n	5	6	7	**8**
$-\Delta T_{\min}/T_0$	0.25	0.26	0.27	**0.278**
$\Delta T_{\max}/T_0$	0.20	0.215	0.228	**0.23**
$\bar{k}_r(T_0)$	0.639	0.600	0.567	**0.539**
$L/\lambda_0(T_0)$	3.25	3.75	4.24	**4.75**
$D/\lambda_0(T_0)$	1.91	2.03	2.15	**2.26**
L/D	1.70	1.85	1.97	**2.10**

a quite large range for temperature variations, without the danger of undesired mode interference. This range can be additionally increased by compensating the wavelength change of the levitator gas with a variable mixture of two gases of extremely different sound velocities as described in [2]. This can be accomplished, for instance, by increasing krypton concentration during heat up, increasing argon concentration during cool down, in combination with automatic pressure release of the gas mixture.

The condition (24) restricts the parameter $\bar{k}_r$ and the length/diameter ratio L/D of Table I to discrete values according to Table II. At $n = 8$ we find a good compromise with $\bar{k}_r = 0.54$, $L/D = 2.1$, $L = 4.75\lambda_0$ and $D = 2.26\lambda_0$. This version has been successfully used in microgravity experiments at 20 kHz [2]. The respective data are therefore in Table I and II marked by bold numbers.

3.5. Required sound intensity and acoustic power

Under *standard-conditions* for safe levitation in air with $\bar{k}_r \approx 0.54$ we find now from equations (18) and (21a,b) for the required sound intensity and the acoustic power the following approximations:

$$\frac{J}{\mathrm{W/cm^2}} \approx \frac{\Phi_s}{1.6}\left[1+17.1\bar{d}_s^3\right]\frac{\lambda_0}{\mathrm{cm}}\frac{\rho_s}{\mathrm{g/cm^3}}, \quad (\bar{d}_s = d_s/\lambda_z < 0.5), \tag{30}$$

$$\frac{P}{\mathrm{Watt}} \approx \Phi_s/2.5\left[1+17.1\bar{d}_s^3\right]\left[\frac{\lambda_0}{\mathrm{cm}}\right]^3\frac{\rho_s}{\mathrm{g/cm^3}} \tag{31}$$

and

$$\frac{P}{m_s}\Big/\frac{\mathrm{W}}{\mathrm{g}} = 17\left[\frac{1+17.1\bar{d}_s^3}{25.1\bar{d}_s^3}\right] \ge 17. \tag{32}$$

Sound intensity and acoustic power increase (cf. Figure 3) proportional to the product of $|1 + 17.1\bar{d}_s^3] \leq \pi$ and sample density ρ_s. The power/mass ratio (32) decreases and reaches its theoretical minimum for spherical samples at the critical diameter $d_{s,\max} = \lambda_z/2$. We recommend however not to exceed $d_{s,\mathrm{opt}} = \lambda_z/3$ as maximum sample diameter, with a respective power/mass ratio $P/m_s \approx 33\,\mathrm{W/g}$.

3.6. A self-tuning tube-levitator with free floating reflector

With known values of the required sound intensity J (30), the respective acoustic power P (31) and the cross section integral (20) of the Bessel-function we can calculate the full levitation force $F(z = 0)$ at the upper pressure antinode of the tube-levitator,

$$F(z{=}0) = \frac{J}{c_0}\frac{7.5}{k_r^2} = \frac{P}{c_0} = M_r g_0. \tag{33}$$

If we replace the rigid tube bottom by an axially free floating, flat reflector of effective mass M_r, the acoustic power P, which levitates samples of mass m_s and $d_s \leq d_{s,\mathrm{opt}} = \lambda_z/3$ – with levitation safety factors $\Phi_s > 1$ – can also balance the reflector weight $M_r g_0$ in a stable equilibrium (see right side of equation 32). This effect is known from *sound pressure scales* [21] and leads with (31), (32) and $1/c_0 g_0 \approx 300\,\mathrm{mg/W}$ in ambient air to a required reflector mass

$$\frac{M_r}{\mathrm{mg}} = \frac{P}{c_0 g_0} \approx 300\frac{P}{\mathrm{W}} \approx 280\left[\frac{\lambda_0}{\mathrm{cm}}\right]^3 \frac{\rho_s}{\mathrm{g/cm^3}}. \tag{34}$$

The tube levitator with self-adjusting reflector provides constant sound intensities at all pressure and velocity antinodes inside the tube, independent of the gas pressure and the front face velocity amplitude of the ultrasonic transducer. The respective levitation safety factor Φ_s for spherical samples with effective diameters $d_s \leq \lambda_z/\pi$ follows from (21a) and (34),

$$\Phi_s \approx 5.5\frac{\bar{k}_r^{1.4}(T_0)}{1 + 17.1\bar{d}_s^3}\left[\frac{T}{T_0}\right]^{0.7}. \tag{35}$$

Under standard conditions with $\bar{k}_r = 0.54$ it varies between $\Phi_s \approx 1.5$ at the optimal and largest tolerated drop diameter $d_s = \lambda_z/\pi$ and $\Phi_s \approx 2.4$ at $d_s \ll \lambda_z/\pi$. A temperature variation according to (35) under consideration of (28) can be tolerated, as long as the levitation safety factor remains slightly above $\Phi_{s,\mathrm{crit}} = 1$. The reflector mass M_r can be changed according to (34) for other sample densities ρ_s and inversely proportional to the factor $\bar{k}_r^{1.4}(T_0)$ according to (35), in case other tube dimensions are to be used.

Table III shows the required reflector mass M_r in milligram (made for example of Balsa wood, or Styrofoam) together with the optimal diameter and mass of levitated water drops and the respective diameter D and length L of the levitator tube for different frequencies. Also shown is the required acoustic power according to equation (34). These data exclude internal losses of the transducer and the power supply.

Table III. Characteristic parameters of a self-tuning levitator according to Figure 4 at different frequencies.

f/kHz	20	30	40	50	**58**
$d_{s,\mathrm{opt}}$/mm	6.4	4.3	3.2	2.6	**2.2**
$m_{s,\mathrm{opt}}$/mg	139	41	17	8.9	**5.7**
M_r/mg	1390	410	170	89	**57**
D/mm	38.4	25.6	19.2	15.4	**13.3**
L/mm	80	54	40	32	**28**
P/W	4.5	1.33	0.56	0.29	**0.185**

3.7. The sound pressure level (SPL)

With the references $p_{\mathrm{ref}} = 2 \cdot 10^{-5}\,\mathrm{N/m^2}$ and $J_{\mathrm{ref}} = 0.966 \cdot 10^{-12}\,\mathrm{W/m^2}$ for the sound pressure amplitude p and the sound intensity J, the *sound-pressure level* SPL can be expressed in logarithmic scale (dB = decibel)

$$\begin{aligned}\frac{\mathrm{SPL}}{\mathrm{dB}} &= 20\log\left[\frac{p}{\sqrt{2}p_{\mathrm{ref}}}\right] = 10\log\left[\frac{J}{J_{\mathrm{ref}}}\right] \\ &\approx 160 + 10\log\left[\frac{J}{\mathrm{W/cm^2}}\right]\end{aligned} \tag{36}$$

with 160 dB being roughly $1\,\mathrm{W/cm^2}$. Because of the low acoustic impedance $Z_0 \approx 430\mathrm{kg/m^2s}$ of air, a free-field sound level around 160 dB would require velocity amplitudes near 7 m/s at the transducer front face. This is close to the dynamic strain limit of high power piezoelectric compound transducers [9]. However, the resonance amplification of the tuned standing wave allows a considerable reduction of the transducer amplitudes. This resonance amplification depends on reflection losses at the solid boundaries and on absorption losses of the levitator gas including leakage openings and absorber targets inside the levitator. In tube levitators according to Figure 2 and in open levitators according to Figure 1 we found a typical amplification $10 < V = p_{\max}/p_{\min} \approx v_{\max}/v_{\min} < 20$, depending on the tube length $L = n\lambda_z/2$.

At very large sample densities ρ_s it might be necessary, to increase the static pressure P_0 inside the levitator tube. This would allow sound intensities (proportional to P_0) of more than $100\,\mathrm{W/cm^2}$ (> 180 dB) [12] without transducer damage.

3.8. Optimal frequency and critical drop size for large drops

The optimal levitation frequency and wavelength in ambient air for large levitated drops with known density ρ_s and surface tension σ_s follows with $\lambda_{z,\mathrm{opt}}/\mathrm{mm} \approx 3d_{s,\max} \approx 400/f\,(\mathrm{kHz})$ from equation (18). The drop diameter is however limited by the critical *Bond number* [3]

$$Bo = g_0\rho_s d_s^2/(4\sigma_s) \leq Bo_{\mathrm{crit}} = 1.4, \tag{37}$$

which correlates the shape stabilizing capillary pressure $4\sigma_s/d_s$ with the destabilizing hydrostatic pressure $\rho_s d_s g_0$. This determines the oblate drop deformation and leads to drop disintegration at $Bo > 1.4$ [3] (cf. Table IV).

Table IV. Critical drop diameter for some representative liquids at $Bo_{\mathrm{crit}} = 1.4$.

Liquid	water	mercury	acetone	benzene	hexane	toluol	methan	CCl_4
$d_{s,\mathrm{crit}}$/mm	6.4	4.4	4.1	4.3	4.2	4.3	4.0	3.1
f_{opt}/kHz	22	31	34	32	33	32	34	45

Table IV shows critical drop diameters of some liquids together with the respective optimal frequencies in ambient air at $\lambda_z/\lambda_0 \approx 1.22$. With the exception of water and CCl_4, 30 kHz seems to be close to optimal for the levitation of drops up to the critical diameter. Smaller drops with $d_s < d_{s,\mathrm{crit}}$ would require smaller sound intensities at higher frequencies. The largest reported water drops, with effective diameters of 6.4 mm and a volume of about 134 µl, have been levitated at 20 kHz [3].

The levitation of extremely small drops with negligibly small inertia is always critical. Small drops are often carried away by asymmetric drag effects of the acoustic convection, or they disappear by fast evaporation (Gibbs-Thomson effect). The smallest reported water drops in a 58 kHz levitator measure 20 µm in diameter. This value can probably be downscaled to about 10 µm at 100 kHz if gases at extremely high humidity are used.

3.9. Typical temperature effects in a standing wave and in levitated drops

The concentration of the acoustic power along the levitator axis (cf. equation 8) leads to a temperature increase $T_0 + \Delta T$ relative to the isothermal background temperature T_0. This temperature increase is proportional to the sound intensity J. It reaches about 3.5 K at $J = 1\,\mathrm{W/cm^2}$ (160 dB) and arrives with a time constant of a few seconds at the centre of large levitated samples. With increasing sound intensity J the linear temperature increase is however more and more counteracted by acoustic convection [2]. In precise drop evaporation measurements the measured *background-humidity* should be corrected by a few percent in consideration of the central acoustic heat up, which is often ignored.

Another considerable temperature effect, leading down to super-cooling, may arise from evaporation, if drops with large vapour pressure and evaporation heat are levitated in dry gases at very low vapour concentration of the drop liquid. If drops of water, ethanol, methanol, benzene or CS_2 respectively are levitated at room temperature [13], this evaporation cooling – not counting the above acoustic heat up - leads to remarkable values: $\Delta T_{\max} \approx -12$ K, -17 K, -20 K, -24 K, -28 K, respectively.

4. Levitation of gas bubbles in water and other liquids

4.1. The liquid-filled tube levitator with "totally reflecting" walls

Because of a better acoustic impedance matching at the solid boundaries of liquid-filled levitator tubes, the reflectivity differs considerably from the total reflection in gas-filled levitators. Depending on the wall thickness and the tube material this may result in wave interferences with complex amplitude and phase relations, combined with increasing absorption losses and changes in the resonance frequencies. Since a correct mathematical description would be too complicated, we will use the simple theory of gas-filled tube-levitators of sections 2 and 3, assuming totally reflecting tube walls for approximations and propose empirical corrections for the resonance fine-tuning.

Liquid-filled levitators with vertical tube axis may be resonance- tuned with an open-end reflecting liquid column of effective length $L = (2n+1)\lambda_z/4$ or with a floating, solid reflector at the top and an effective tube length $L = n\lambda_z/2$. In both cases the reflector has to be readjusted for the resonance fine-tuning. Wavelengths in liquids and resulting tube dimensions are larger by a factor 5 as compared with gas levitators of the same frequency. This considerably changes the tube dimensions at the same frequency.

In order to avoid undesired interferences between 0/1-Bessel-mode (λ_z) and longitudinal wave (λ_0) we apply equations (24) through (27) with $n = 5$ and $m = 7$ and find for the open-end reflector $L = 4\lambda_0$ with $\bar{k}_r = 0.726$ and $D = 1.68\lambda_0$. A solid reflector would lead with $L = 3.75\lambda_0$ to $\bar{k}_r = 0.745$ and $D/\lambda_0 = 1.638$.

A schematic cut view of a typical, water-filled tube levitator is shown in Figure 4. The piezoelectric compound transducer [9] with a diameter $D_T \approx \lambda_0/2$, is epoxy-cemented to a stainless steel membrane at the tube bottom. The dark attraction zones with $\bar{U} < 0$ at the pressure nodes of Figure 2 have completely disappeared, because equations (2a,b) lead to $f_2 = 3 \ll |f_1|$ (cf. section 4.3). The energy potential is dominated by ellipsoidal radiation pressure maxima with aspect ratios $a : b = 3 : 2$ and levitation-force ratios $F_{r,\max}/F_{z,\max} \approx 3 : 4$ (cf. equation 41b) at the sound pressure antinodes.

4.2. The volume resonance of pulsating gas bubbles

Gas bubbles have – contrary to drops and particles – a large compressibility. They change their volume inversely proportional to the hydrostatic pressure P_0 and additionally by diffusive gas exchange with the surrounding liquid/gas solution. Under periodic acoustic pressure variation $p = p_0 \cos \omega t$ their diameter $d_s(t) = d_{s,0}(P_0) + \Delta d(\bar{d}_s, p) \cos(\omega t - \varphi)$ with $\bar{d}_s = d_s/d_{s,r}$ will periodically change. In this bubble pulsation the compressed gas volume and the displaced liquid mass counteract as spring-mass-system with a volume-resonance at a given average

bubble diameter [14]

$$\frac{d_{s,r}(f)}{\mathrm{mm}} \approx \frac{1}{\pi f}\sqrt{3\frac{\kappa_g}{\rho_w}\left[P_0 + \frac{3\kappa_g - 1}{3\kappa_g}\frac{4\sigma_w}{d_s}\right]} \approx \frac{6.5}{f/\mathrm{kHz}}\sqrt{\frac{P_0}{\mathrm{bar}}}. \quad (38)$$

The resonance diameter depends on frequency f, hydrostatic pressure P_0, density ρ_w of the liquid (water) and on the specific heat ratio of the gas $\kappa_g(\mathrm{air}) = c_v/c_p = 1.4$. The increasing capillary pressure requires corrections for small bubble diameters.

4.3. The characteristic factors f_1 and f_2 of a vibrating bubble and resulting levitation force profiles

A pulsating bubble of normalized average diameter $\bar{d}_s = d_s/d_{s,r}$ will change its relevant reflecting cross section during growth or shrinkage through the resonance curve (38). This results in a strong influence of $\bar{d}_s$ on the positioning forces in a standing-wave levitator. The characteristic factor f_1 in the potential equation (8) is not a constant anymore, but strongly varies with changing bubble diameter $\bar{d}_s$. Yosioka and Kavasima [15] have calculated and measured the positioning forces of air bubbles in water, by using plane standing waves with horizontal wave fronts and node lines. Because plane standing waves allow a free bubble movement in lateral direction, they are not suited for stable multi-axial positioning. We can however derive the required sound intensity for the levitation of bubbles in a Bessel-mode tube levitator, if we introduce the findings of [15] into our mathematical concept of equations (2a,b) and (18). We find agreement for $f_2 = 3$ and a strong difference for f_1, represented by the factor in large brackets of equation (39),

$$f_1 = 1 - \frac{\rho_w c_w^2}{\rho_g c_g^2}\left[\frac{2}{3}\frac{\rho_w/\rho_g}{\bar{d}_s^2(1-\bar{d}_s^2)}\right] \approx \frac{7.75\cdot 10^6}{\bar{d}_s^2(\bar{d}_s^2-1)}\left[\frac{P_0}{\mathrm{bar}}\right]^{-2} \quad (39)$$

(index: w - water, g - gas).

The introduction of $|f_1| \gg f_2$ from (39) into (18) leads to attraction potentials $\bar{U} < 0$ at the pressure antinodes for small bubbles with $\bar{d}_s < 1$ (cf. Figure 4). The respective potential distribution (18) results – at typical values $\bar{k}_r = 0.75$, $d_s \ll \lambda_z$ and $\Phi_s = 1.5$ – in axial levitation forces with the respective sound intensities J and pressure amplitudes p approximated by (cf. lopes at the left of the resonance minima in Figure 5)

$$\frac{J}{\mu\mathrm{W/cm^2}} \approx \bar{d}_s^2(1-\bar{d}_s^2)\frac{\lambda_z}{\mathrm{cm}}\left[\frac{P_0}{\mathrm{bar}}\right]^2 \quad (40a)$$

and

$$\frac{p}{\mathrm{mbar}} \approx \sqrt{3\bar{d}_s^2\left|1-\bar{d}_s^2\right|\frac{\lambda_z}{\mathrm{cm}}}\frac{P_0}{\mathrm{bar}} \le \frac{11P_0/\mathrm{bar}}{\sqrt{f/\mathrm{kHz}}} \quad (40b)$$

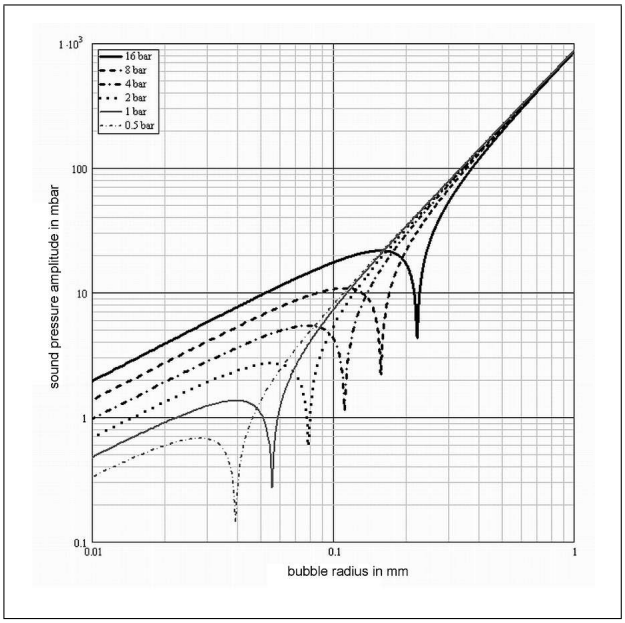

Figure 5. Required sound pressure amplitudes (40b) for the levitation of air bubbles in water at 58 kHz as functions of the bubble radius (in mm) with the hydrostatic pressure P_0 (0.5; 1; 2; 4; 8 and 16 bar from the left) as parameter.

Near the pressure antinodes of the water-filled tube levitator of Figure 4 we can therefore levitate small bubbles with $\bar{d}_s < 1$ at ambient pressure ($P_0 = 1$ bar) and frequencies between 20 and 60 kHz with extremely small sound pressure amplitudes around 1 mbar or sound intensities below 1 μW/cm^2.

In the relevant parameter range $0 \le \bar{k}_r \le 0.75$ we find from (9) and (13b) instead of (23a,b)

$$\frac{F_{z,\max}(\bar{k}_r)}{F_{z,\max}(0)} \approx \sqrt{1-\bar{k}_r^2} \quad (41a)$$

and

$$\frac{F_{r,\max}(\bar{k}_r)}{F_{z,\max}(0)} \approx \frac{2}{3}\frac{\bar{k}_r}{\sqrt{1-\bar{k}_r^2}}. \quad (41b)$$

4.4. Levitation of "large bubbles" with diameters above volume resonance

Because of the sign change in equation (40a) for bubbles with $\bar{d}_s > 0$, the potential minima at the dominant sound pressure antinodes of Figure 4 will turn into repulsive maxima ($\bar{U} > 0$). Large bubbles with $\bar{d}_s > 1$ will therefore be pushed to the periphery of the tube, where they freely rise to the surface. The missing centralizing radial forces can however be realized by a "doughnut shaped" radiation pressure profile with concave central minimum above the bubble [7]. If the axial force component at this central minimum is strong enough, it will compensate the effective buoyancy of the rising bubble according to equation (41). The required acoustic pressure amplitudes are shown in the increasing slopes at the right of the resonance minima in Figure 5.

Table V. Optimal dimensions of a water-filled cylindrical tube levitator for large bubbles. (1) Solid reflector, (2) free liquid level.

	(1)	(2)	(1)	(2)	(1)
L/λ_0	1.50	1.75	2.00	2.25	2.50
D/λ_0	3.42	3.50	4.00	5.17	5.54
D/L	2.28	2.00	2.00	2.26	2.18
L(58kHz)/cm	3.90	4.55	5.20	5.85	6.50
D(58kHz)/cm	8.85	9.10	10.40	13.2	14.20

In a half-empirical approach for the calculation of a doughnut shaped radiation pressure profile we used a short, open-end liquid column with $L \approx 1.75\lambda_0$, a relatively large tube diameter $D \approx 2L$ and a transducer diameter $D_{\mathrm{tr}} = \lambda_0/2$ with a sound pressure directivity characteristics

$$\Psi(\varphi) = \frac{2J_1(0.5k_0 D_{\mathrm{tr}} \sin\varphi)}{0.5k_0 D_{\mathrm{tr}} \sin\varphi} = \frac{2J_1(\pi/2 \sin\varphi)}{\pi/2 \sin\varphi}. \quad (42)$$

The sound pressure amplitudes $p(r, z)$ at any point with the coordinates $0 \le r \le R$ and $0 \le z \le L$ are described by a convergent series of beams, emerging from the centre of the radiating transducer under the angles φ against the vertical tube axis, with

$$0 \le \varphi = \arctan\left[\frac{2\nu R - r}{2\mu p L - z}\right] \le \pi/2, \quad (43)$$

$\mu, \nu = 1, 2, 3,$ etc. having the effective lengths

$$X_{\mu,\nu}(r, z) = \sqrt{(2\mu L - z)^2 + (2\nu R - r)^2}. \quad (44)$$

Each point within the water-filled tube is reached either directly ($\mu = 0$ and $\nu = 0$) or after μ reflections at the free liquid surface and ν reflections at the solid tube wall. The pressure amplitudes of the components are inversely proportional to the distances $X_{\mu,\nu}(r, z)$. Considering the phase factors $\cos(k_0 X_{\mu,\nu}(r, z))$ and the directivity characteristics (42) we find for the normalized sound pressure amplitudes $\bar{p}(r, z)$:

$$\bar{p}(r, z) = \sum_{\mu=0}(-1)^{\mu} \sum_{\nu=0} \frac{\cos\left(k_0 X_{\mu,\nu}(r, z)\right)}{X_{\mu,\nu}(r, z)} \frac{2J_1\left((\pi/2)\sin\varphi\right)}{(\pi/2)\sin\varphi}$$

$$= \frac{4}{\pi} \sum_{\mu=0}(-1)^{\mu} \sum_{\nu=0} \frac{\cos\left(k_0\sqrt{(2\mu L - z)^2 + (2\nu R - r)^2}\right)}{2\nu R - r} \cdot J_1\left(\frac{(\pi/2)(2\nu R - r)}{\sqrt{(2\mu L - z)^2 + (2\nu R - r)^2}}\right). \quad (45)$$

The factor $(-1)^{\mu}$ for the resonance distance $L = (2n + 1)\lambda_0/4$, with a pressure node at the free liquid surface, represents the phase shift ($\cos\pi = -1$), if a beam is reflected (μ-times) at the liquid/gas interface (cf. Figure 6a). This factor disappears, if a solid top-reflector, for instance a transparent glass plate, is used (cf. Figure 6b). In this case the pressure antinode at $z = L$ requires a resonance distance $L = n\lambda_0/2$ to the transducer front face. This version has the advantage of an easy access for observation and undisturbed optical measurements at the smallest possible distance between the levitated bubble and a transparent top reflector.

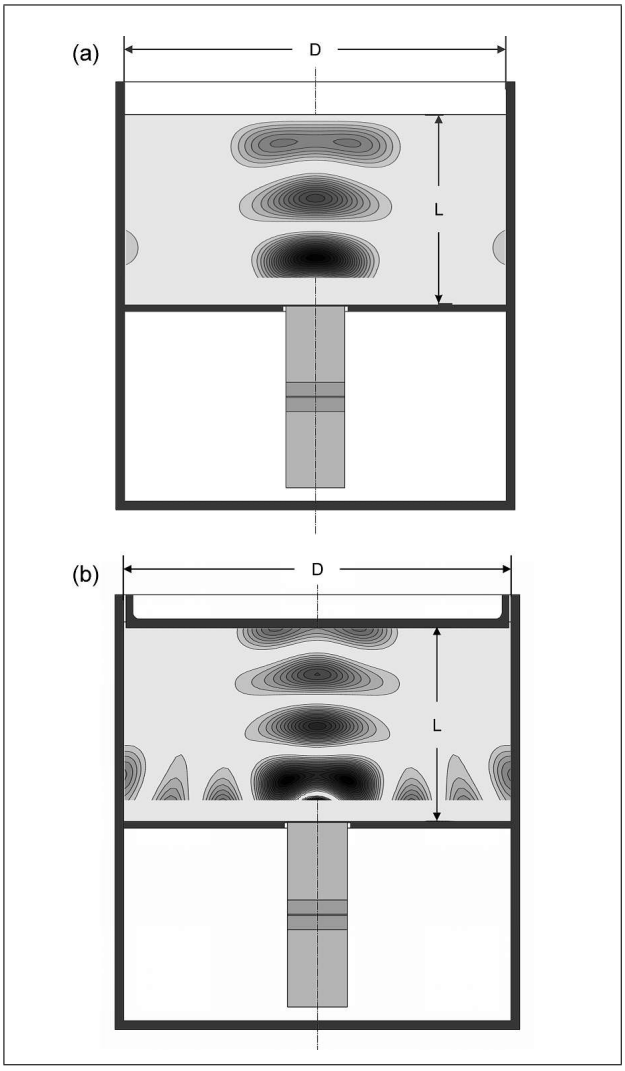

Figure 6. (a) Normalized radiation pressure profile in a water filled cylindrical tube levitator with free reflecting liquid level for the positioning of large gas bubbles ($\bar{d}_s > 1$) underneath the ring profile and of small bubbles ($\bar{d}_s < 1$) at the central maximum below $\lambda/2$. $D = 2L = 3.5\lambda_0$. (b) Normalized radiation pressure distributions in a water filled cylindrical tube levitator with floating, solid top reflector for the positioning of large gas bubbles ($\bar{d}_s > 1$) underneath the ring profile and of small bubbles ($\bar{d}_s < 1$) at the central maximum $\lambda_0/2$ below. $D = 2L = 4\lambda_0$.

Optimal results of our calculation of normalized radiation pressure profiles are summarized in Table V. With $0 \le \mu, \nu \le 2$ we used 25 convergent beam components for each point with the coordinates r and z. Figures 6a,b are design examples for $L = 1.75\lambda_0$ and $L = 2\lambda_0$ at the standard frequency of 58 kHz. All radiation pressure profiles have an axial-symmetric, concave shape near the top reflector, which allows the positioning of large bubbles with $\bar{d} > 1$ at constant levitation safety factor $\Phi_s = 1$.

4.5. Position change of levitated bubbles during growth through the volume resonance

Figures 6a,b show also radiation pressure profiles at the central pressure antinodes in $\Delta L = n\lambda_0/2$ axial distance underneath the ring profile. The upper one has a radiation pressure maximum, by a factor 2 larger than the central ring minimum in Figure 6a and by a factor 2.5 larger in Figure 6b. These radiation pressure maxima are perfectly suited for the levitation of small bubbles with $\bar{d} < 1$. In the same way as in the Bessel-mode tube of Figure 4 their levitation safety factor $\Phi_s \geq 1$ can be increased proportional to the sound intensity at nearly constant bubble position.

If a small levitated bubble with $\bar{d}_s < 1$ grows (e. g. by gas diffusion) beyond the critical diameter $\bar{d}_s = 1$, it will be automatically released from the central radiation pressure maximum into the ring centre above, where its buoyancy is compensated by the concave, centralising radiation pressure profile (cf. Figure 6a,b) The characteristic radiation pressure profile around a levitated large bubble provides large radiation pressure at the upper halve sphere and considerably smaller radiation pressure at the lower halve sphere. This is quite different from the nearly spherical symmetry of small bubbles at the pressure antinode underneath. If the acoustic power is increased, the large bubble – in contrast to the small bubble – will change its position downwards, until a new equilibrium at constant $\Phi_s = 1$ is reached.

4.6. Example of an optimized bubble levitator

At the standard frequency $f = 58\,\mathrm{kHz}$, with a wave length $\lambda_0 = 2.6\,\mathrm{cm}$ in water and a transducer diameter $D_{\mathrm{tr}} = \lambda_0/2 = 1.3\,\mathrm{cm}$ the optimized levitator with free reflecting liquid level according to Figure 6a would require a tube diameter $D_a = 9.1\,\mathrm{cm}$ and a respective tube length $L_a = 4.55\,\mathrm{cm}$, with a ring diameter of about $0.6\lambda = 1.6\,\mathrm{cm}$. The optimized version with solid top reflector according to Figures 6b requires $D_b = 10.4\,\mathrm{cm}$ and $L_b = 5.2\,\mathrm{cm}$. The diameter of the ring profile is here larger and close to one wave length $\lambda_0 = 2.6\,\mathrm{cm}$. Bubbles with diameters $d_s < 112\,\mu\mathrm{m}$ will be levitated near the central pressure antinode underneath the ring profile. They are released from this pressure antinode, if $d_s \geq 112\,\mu\mathrm{m}$ and automatically stopped in their uprising at the centre of the ring profile. The required sound intensity and sound pressure amplitude at the ring centre follow from equations (40a) and (40b) and lead to a steep increase for $\bar{d}_s^2 \gg 1$ independent of the hydrostatic pressure P_0 with

$$\frac{J}{\mathrm{mW/cm^2}} \approx 16.4\left[\frac{d_s}{\mathrm{mm}}\right]^4\left[\frac{f/\mathrm{kHz}}{58}\right]^3 \tag{46}$$

and

$$\frac{p}{\mathrm{mbar}} \approx 222\left[\frac{d_s}{\mathrm{mm}}\right]^2\left[\frac{f/\mathrm{kHz}}{58}\right]^{1.5}. \tag{47}$$

A tolerable sound intensity $J = 1\,\mathrm{W/cm^2}$ with respective sound pressure amplitude $p = 1.74\,\mathrm{bar}$ at the ring centre are therefore sufficient to levitate bubbles with diameters $d_s \leq 2.8\,\mathrm{mm}$ in a 58 kHz levitator or with diameters $d_s \leq 6.2\,\mathrm{mm}$ in a 20 kHz levitator according to Figures 6a,b.

5. Summary and conclusion

Section 2 concentrates on a short review of the theory of ultrasonic standing waves in cylindrical Bessel-mode tubes, with design criteria, based on axial/radial levitation forces, the selection of optimal geometrical proportions and power requirements for fluid (gas or liquid) carrier medium in general. Section 3 applies the theory to drops and particles, with effective diameters $d_s \leq \lambda/2$ between about 20 µm and 6 mm, in gas levitators at frequencies from 20 kHz to 100 kHz. The best frequency of a levitator is determined by the ratio $d_{s,\max}/\lambda \approx 1/3$ of the largest desired drop/particle diameter and the wave length λ. Special attention has been given to the suppression of mode interference at variable temperature, to drop size limitation at the critical Bond number and to temperature effects, caused by acoustic heat up, acoustic convection and drop evaporation. Section 4 deals with the levitation of gas bubbles in liquid/gas solutions, with characteristic resonance phenomena during growth or shrinkage. It identifies the volume resonance as a critical parameter to distinguish between *small bubbles*, which can easily be levitated in the sound pressure antinodes of a standing wave – and *large bubbles*, which need a special ring-type pressure profile as described in Figures 6a,b.

An appendix – for readers of special interest – introduces the effect of capillary wave resonances at the surface of pulsating gas bubbles as an interesting topic for detailed investigations with a standing wave levitator. This would allow the observation of the generation of microbubbles, which have a considerable nucleation effect on acoustic cavitation, degassing and aerosol atomization. A possible explanation for the sudden death of whales near strong sonar systems is sketched by applying the theory under realistic assumptions at carrier frequencies between 2 and 8 kHz.

Appendix: Capillary-wave cavitation at the surface of pulsating bubbles in gas-oversaturated liquids

A1. Radial displacement amplitudes of pulsating bubbles

The levitators in Figures 6a,b offer a chance for detailed investigations of some interesting effects in connection with capillary waves at the surface of freely pulsating, stationary gas bubbles in water and other liquids.

The displacement amplitudes Δr of radial bubble pulsations depend on the effective sound pressure amplitude p, the hydrostatic pressure P_0 and the normalized diameter $\bar{d}_s = d_s/d_{s,r}$ of the resonance curve (38). For small radial displacements $\Delta r/r_s$ we can assume linear pulsations and find from [14]

$$\Delta r = \frac{p/2\pi f}{\sqrt{3\kappa_g \rho_L P_0}} \frac{1}{\sqrt{(\bar{d}_s - 1/\bar{d}_s)^2 + (\bar{d}_s/Q)^2}}. \tag{A1}$$

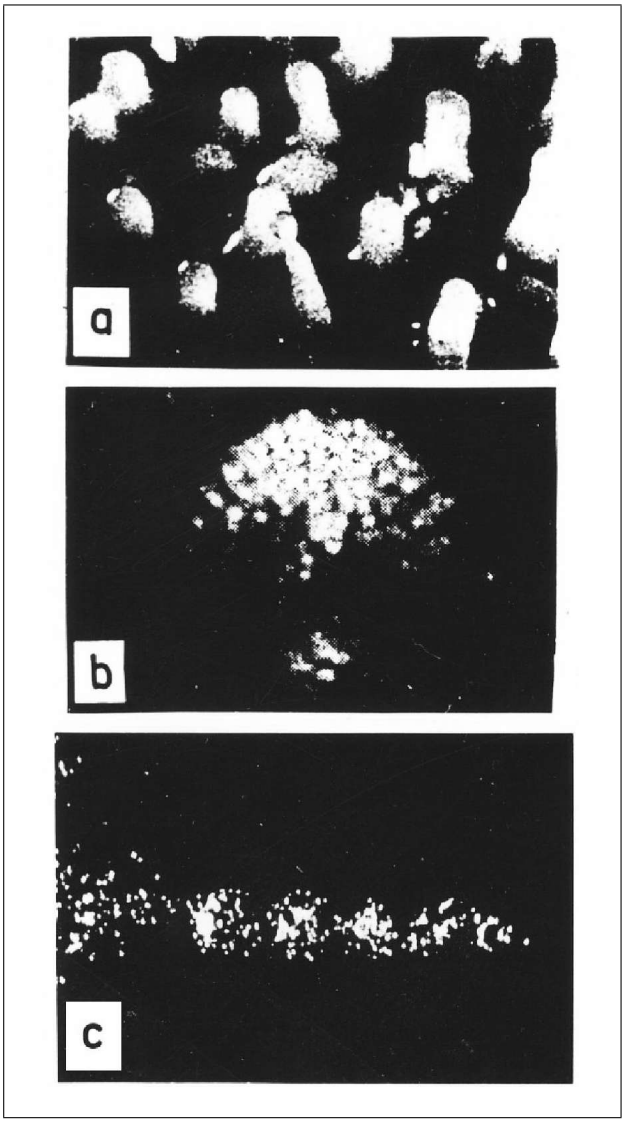

Figure A1. Capillary waves after Lierke [14]: (a) on a plane interface, (b) on a gas bubble with 3.6 mm diameter in water at 20 kHz, (c) generation of mikrobubbles at 20 kHz with $d_s < d_{s,r}$. Bubbles were fixed on a porous, sound transmissive rubber plate and fotographed with 6 µs.

This leads – with $\kappa_g = 1.4$ (gas,air) and $\eta_L = \eta_W = 10^{-3}$ Ns/m^2 (dynamic viskosity of liquid/water) – to a resonance curve of the reqired pressure amplitude

$$\frac{p(\Delta r)}{\text{mbar}} \approx 1.3 \frac{f}{\text{kHz}} \frac{\Delta r}{\mu\text{m}} \sqrt{\frac{P_0}{\text{bar}}} \sqrt{\left(\bar{d}_s - \frac{1}{\bar{d}_s}\right)^2 + \left(\frac{\bar{d}_s}{Q}\right)^2} \geq 1.3 \frac{f}{\text{kHz}} \frac{\Delta r}{\mu\text{m}} \frac{\sqrt{P_0/\text{bar}}}{Q}, \quad \text{(A2)}$$

with the quality factor

$$Q = \frac{3}{8\pi} \frac{\kappa_g}{\eta_L} \frac{P_0}{f} \approx \frac{10^5}{6} \frac{1}{\bar{\eta}_L} \frac{P_0/\text{bar}}{f/\text{kHz}}, \quad \text{(A3)}$$

and $\bar{\eta}_L = \eta_L/\eta_W$ as viscosity ratio.

A2. Surface wave excitation and atomization of micro-bubbles

The surface of a pulsating bubble in water becomes instable at characteristic bubble diameters $d_s(n)$ and frequency-dependent displacement-amplitudes $\Delta r(f) > 1.2\,\mu\text{m} \cdot (20\,\text{kHz}/f)^{1/3}$ [16]. It shows a ripple of crossed surface- or *capillary waves*, which can be described by *spherical functions* of the order n [14]. At $n \geq 2$ the circumference $\pi d_s(n)$ of the bubble is close to a multiple number $n\lambda_K$ of the capillary wave length (cf. right side of equation A4)

$$\frac{\lambda_K}{\text{mm}} \approx 2\sqrt[3]{\frac{\sigma_L \pi}{\rho_L f^2}} \approx \frac{1.23}{[f/\text{kHz}]^{2/3}} \approx \frac{\pi d_s(n)/n}{\sqrt[3]{(1-1/n)(1+1/n)(1+2/n)}}. \quad \text{(A4)}$$

The capillary wave length is proportional to the frequency $f^{-2/3}$ and in water, with the surface tension $\sigma_L = \sigma_W = 74 \cdot 10^{-3}$ N/m, has a corresponding value $\lambda_K(60\text{kHz}) \approx 80$ µm.

With increasing acoustic pressure- and radial displacement amplitudes Δr the capillary-wave amplitudes grow until, at a critical value [16]

$$\Delta r \geq \Delta r_{\text{crit}} = 7\,\mu\text{m}(20\text{kHz}/f)^{1/3}(\eta_L/\eta_W)^{1/6} \quad \text{(A5)}$$

an increasing number of *micro-bubbles* with the average diameter $d_s^* \approx \lambda_K/4$ separate from the surface of the "mother-bubble". The effect may be called *capillary-wave cavitation* (cf. Figure A1) and requires for air bubbles in water radial displacement amplitudes of about 7 µm at 20 kHz, 6 µm at 30 kHz and 5 µm at 60 kHz.

With equation (A4) and the known diameter $d_{s,r}$ of the volume resonance (38) we find from

$$n^* \sqrt[3]{(1-1/n^*)(1+1/n^*)(1+2/n^*)} \approx n^* \approx 16.6 \frac{\sqrt{P_0/\text{atm}}}{\sqrt[3]{f/\text{kHz}}} \quad \text{(A6)}$$

critical numbers $n^*(P_0, f)$ as functions of the hydrostatic pressure P_0 at given frequency f (cf. Table A1). At these numbers volume resonance and surface resonance of the order $n = n^*$ are in coincidence. Surface resonances of "mother-bubbles" with $n = n^* - \nu$ ($\nu = 1, 2, 3$), at the left side, are separated from surface resonances with $n = n^* + \nu$ ($\nu = 1, 2, 3$), at the right side of the volume resonance-diameter. Small "mother-bubbles", with $\bar{d}_s(n) < 1$, are attracted by the pressure antinodes of a standing wave and remain there, if the sound pressure amplitude is above the critical levitation level (40b) with the levitation safety factor $\Phi_s \geq 1$. Therefore their radial displacement amplitude Δr can be varied proportional to the sound pressure (A1) until microbubbles with diameters around 20 µm at 60 kHz or around 30 µm at 30 kHz are generated. The respective sound pressure amplitudes follow with (A2) through (A6),

Table A1. Number n^* of surface resonance at the volume resonance with bubble diameter $d_{s,r}$ in mm as function of the hydrostatic pressure P_0 in bar at three different frequencies according to equation (A6).

	n^*	2	3	4	5	6	7	8	9	10	11	12	13	14	15	16
20kHz	P_0	0.14	0.32	0.54	0.82	1.14	1.56	1.96	2.45	3.00	3.60	4.25	4.95	5.75	6.60	7.50
	$d_{s,r}$	0.11	0.18	0.24	0.30	0.35	0.41	0.46	0.51	0.57	0.62	0.67	0.73	0.78	0.84	0.90
40kHz	P_0	0.22	0.51	0.86	1.30	1.81	2,48	3.11	3.89	4.76	5.71	6.74	7.86	9.12	10.3	11.9
	$d_{s,r}$	0.08	0.12	0.15	0.19	0.22	0.26	0.29	0.32	0.36	0.40	0.43	0.46	0.49	0.52	0.56
60kHz	P_0	0.29	0.67	1.12	1.71	2.47	3.24	4.08	5.10	6.24	7.49	8.84	10.3	12.0	13.7	15.6
	$d_{s,r}$	0.06	0.09	0.11	0.14	0.17	0.19	0.22	0.24	0.27	0.30	0.32	0.35	0.37	0.40	0.43

Table A2. Critical sound pressure amplitudes for micro-bubble generation in blood at 2 kHz (8 kHz).

Hydrostatic pressure P_0/bar		1.6	3.5	6.2	9.5	
Repective water depth /m		6	25	52	85	
Surface mode number n^*		16 (10)	24 (15)	32 (20)	40 (25)	prop. $\sqrt{P_0}/\sqrt[3]{f}$
Volume resonance diameter	$d_{s,r}(n^*)$/mm	4 (1)	6 (1.5)	8 (2)	10 (2.5)	prop. $\sqrt{P_0}/f$
Minimum sound pressure	$p_{\min}(n^*)$/µbar	20 (200)	13.3 (133)	10 (100)	8 (80)	prop. $f^{5/3}/\sqrt{P_0}$
Minimum sound pressure at $n^* \pm \nu$	p_ν/mbar	$\approx 7.5 f/2\nu$ for $\nu = 1, 2, 3, \ldots$ and all pressures P_0				
Resulting bandwidth	B_ν/mm	$\approx \pm\nu/(2f)$ for $\nu = 1, 2, 3, \ldots$ and all pressures P_0				

$\bar{d}_s = n/n^*$ and $\nu = 1, 2, 3 \ll n^*$ from

$$\frac{p(n^* \pm \nu)}{\text{mbar}} \approx 1.3 \frac{f}{\text{kHz}} \frac{\Delta r_{\text{crit}}}{\mu\text{m}} \sqrt{\frac{P_0}{\text{bar}}} \left| \frac{n}{n^*} - \frac{n^*}{n} \right| \approx 7.5\nu \frac{f/2}{\text{kHz}} \left(1 \mp \frac{\nu/2}{n^*}\right) \approx 7.5\nu \frac{f}{2}. \quad \text{(A7a)}$$

The ratio of equations (A7a) and (40b) leads to the approximation

$$\Phi_s(n) \approx 0.4 \left[\frac{f}{\text{kHz}}\right]^{4/3} \left[\frac{P_0}{\text{bar}}\right]^{-3/4} \cdot \left[\bar{\eta}\right]^{1/6} \sqrt{\nu} \left(1 \pm \frac{3}{4} \frac{\nu}{n^*}\right) \quad \text{(A7b)}$$

for the associated levitation safety factor $\Phi_s(n)$ at the critical level for micro-bubble generation, with the + sign at the left and the − sign at the right side of the volume resonance (n^*).

Large "mother bubbles" with $\bar{d}_s(n) > 1$ are repelled from the pressure antinodes and rise to the surface, unless they are stopped by radiation pressure rings as shown on top of Figures 6a,b. Their stabilizing acoustic pressure is however – in contrast to the spheroidal symmetry of "small" mother-bubbles in the pressure antinodes – concentrated around the top region of the bubbles. With increasing sound pressure they change their position downwards at constant levitation safety factor $\Phi_s = 1$. Therefore pulsation amplitudes, required for surface waves of sufficient displacement amplitude (A5) can hardly be excited.

The number of microbubbles, generated by capillary wave cavitation in standing waves, grows proportional to the square of the number $n^*(P_0, f)$ (cf. Table A1). Large n^*-numbers may even lead to permanent surface-resonance by resonance-overlapping of different surface modes with $n \leq n^*$. In transient, non-standing ultrasonic waves – as assosiated with sonar systems in the audible frequency range - both, "small" and "large" mother-bubbles with surface resonances at n^*, $n^* \pm 1$, $n^* \pm 2$, etc. can eventuelly reach the required radial displacement amplitudes (cf. section A5).

A3. Bjerknes forces between pulsating bubbles

Microbubbles in the vicinity of pulsating mother-bubbles initiate interesting hydrodynamic interactions by *Bjerknes forces* [17], which could be studied, if the mother-bubbles are stably positioned. *Bjerknes* forces have their theoretical analogy in *gravity forces* between planets or in *Coulomb forces* $f_C = q_1 q_2 / L^2$ between electrically charged drops or particles at a short central distance L. The unipolar or bipolar charges q_1 and q_2 have only to be replaced by the velocities $\mathrm{d}(m_1)/\mathrm{d}t$ and $\mathrm{d}(m_2)/\mathrm{d}t$ of the displaced liquid mass-change during the radial bubble pulsation, with respective phase angles Φ_1 and Φ_2. Small mother-bubbles pulsate in phase with the generated microbubbles ($\cos(\Phi_1 - \Phi_2) > 0$), while large mother-bubbles pulsate in counter-phase ($\cos(\Phi_1 - \Phi_2) < 0$). This leads in the first case to attraction forces with direct recombinations or complicated microbubble circulations, or to a visible "corona" around the mother bubble. In the second case – which can be observed in progressing waves with mechanically fixed mother-bubbles [14] – the microbubbles will be repelled by the mother-bubble and rise to the surface of the liquid.

A4. Some applications of capillary wave cavitation

The effect of capillary-wave cavitation has a strong influence on some technical ultrasonic applications. Ultrasonic degassing of oversaturated gas solutions [14] for instance

can rapidly increase, if the capillary waves at the surface of a few resonance bubbles initiate a permanent nucleation. The effect is self-sustained, because the volume loss of the mother-bubbles by microbubble-generation can be effectively compensated by rapid diffusion growth from the oversaturated gas solution. The generation of aerosols with ultrasonic geyser atomizers at MHz frequencies [18] is another example. It requires countless microscopic gas bubbles in volume resonance, with capillary waves at their surface. This has been demonsrated after extreme degassing of the liquid, which results in a total suppression of the atomization. These resonance bubbles also explain the measured, strong correlation between the average aerosol diameter and the capillary wavelength ($d(f) \approx f_K/4 \propto f^{-2/3}$). The bubbles act as transient amplifiers and lead to the required large displacement amplitudes before they burst at the free surface of the gyser.

A5. Capillary wave cavitation, a possible explanation for the sudden death of whales?

Capillary wave bubble resonances with drastically increasing gas bubble nucleation may also contribute to the explanation of the sudden death of whales [19], which are often hit by powerfull military sonar systems. The animals are irritated by strong and strange noise and try to escape into shallow water with static pressures P_0 of a few atmospheres. After rapid surfacing from large water depth, with highly gas oversaturated blood, the capillary wave cavitation in progressing acoustic waves – especially at low frequency (cf. equation (A1) through A5) – can trigger a rapid "cold boiling" of the blood and destroy important blood vessels and organs by gas- and fat emboly. This would however require sound pressures of sufficient amplitudes in a realistic distance $r \leq 1$ km from the SONAR system.

Modern middle-frequency sonar systems emit far reaching, frequency-modulated sound beams at carrier-frequencies between 2 and 8 kHz with pressure levels of more than 235 dB (ref. 1 µPa) respectively [19]. This is equivalent to near-field sound pressure amplitudes $p(N) = 0.56$ MPa = 5.6 bar at about 1 to 2 m distance. The sound pressure at a radial distance $r \gg N \approx D^2/4\lambda$ in the far-field of a transducer with the diameter D and the near-field length N, can be described by

$$p(r,\varphi) \approx p(N)\sin\left(\frac{\pi}{2}\frac{N}{r}\right)\frac{2J_1(\pi D/\lambda\sin\varphi)}{\pi D/\lambda\sin\varphi} \cdot \exp\left[-\alpha(f)\left(r-N\right)\right] \leq p(N)\frac{\pi\lambda}{8r}\left(\frac{D}{\lambda}\right)^2 \quad \text{(A8)}$$

The Bessel function $|2J_1(x)/x] \leq 1$ in the centre of (A8) is the *directivity* factor of the beam, with its central maximum at $\varphi = 0$

Typical acoustic absorption losses $\alpha(f)$ in seawater at 2 °C and 10 bar, ranging from 0.1 dB/km at 2 kHz to about 0.9 dB/km at 8 kHz, are negligible as compared with the losses by beam spreading. The same applies to reflection losses at the – impedance matched – animal (fish) / water interface and for absorption losses inside the body of the animal (fish). The dominant spreading losses (at the right of equation A8) depend on the ratio D/λ of the transducer-diameter D at given wavelength λ. If we assume a sound pressure amplitude $p(N) = 5.6$ bar at a realistic near-field-distance $N = 2$ m of a 2 kHz sonar transducer with $\lambda = 0.75$ m, equation (A8) would lead to realistic axial sound pressure amplitudes

$$p(r,\varphi)/\text{mbar} = p(r,0) \approx 18/r, \quad \text{(A9)}$$

with r measured in km.

We try now to estimate the possibilities for capillary-wave cavitation on gas-bubbles in blood $\eta_L/\eta_W \approx 4$ at 2 kHz and local sound pressures < 50 mbar.

We use four different hydrostatic pressures between 1 and 10 bar ($\leq$ 100 m sea-level depth) as parameter. If we apply equations (38) and (A1) through (A6), we find from (A5) critical radial displacement amplitudes $\Delta r_{\text{crit}} \approx 20$ µm for the generation of micro-bubbles in blood with typical diameters $d_s^* \approx \lambda_K/4 \approx 0.2$ mm. They can be atomized from "mother-bubbles" with volume-resonance diameters $d_{s,r}/\text{mm} \approx 3.25\sqrt{P_0/\text{bar}}$ according to equation (38). The respective sound pressure amplitudes at coinciding volume- and surface resonances $n^* = 13\sqrt{P_0/\text{bar}}$ (A6) are according to (A2) $p_{\min}/\text{mbar} \approx 4n^*/Q \approx 0.32/n^* \ll 1$. Neighbouring surface resonances at $n = n^* \pm \nu$, with $\nu = 1, 2, 3$ and bubble diameters $d_s(n)/\text{mm} \approx n\lambda_K/\pi \approx n/4$ according to (A4) require respective sound pressure amplitudes according to (A7a). This leads –at 2 kHz– to critical sound pressure amplitudes $p_1 \approx 7.5$ mbar, $p_2 \leq 15$ mbar and $p_3 \approx 22.5$ mbar, with associated diameter-bandwidths (around $d_s(n)$): $B_1/\text{mm} = \pm 0.25$, $B_2/\text{mm} = \pm 0.5$ and $B_3/\text{mm} = \pm 0.75$. The results of our calculation are summarised in Table A2.

The low sound pressure amplitudes $p_{\min}(n^*) < 0.2$ mbar are out of consideration, because of a too narrow bandwidth. The other surface resonances at $n^* \pm \nu$ require sound pressure amplitudes below 50 mbar for 2 kHz and below 200 mbar for 8 kHz, up to $\nu \leq 6$, independend of the hydrostatic pressure $P > 0$. They have sufficiend diameter-bandwidths. This is close to the estimated range of the sound pressure amplitude in up to 1 km distance of a sonar transducer with a nearfield length $N = 2$ m, according to equation (A9). Less critical values for higher frequencies can be determined from Table A2.

Our calculations identify the effect of capillary-wave cavitation, followed by rapid degassing as one possible explanation for the sudden death of whales near strong sonar systems. They also show, that the probability for rapid degassing of oversaturated blood by acoustic micro-bubble generation decreases with increasing frequency. The effect depends however on the existence of at least some bubbles, that have grown – by hydrostatic pressure release, gas diffusion and agglomeration – to the critical range of the pressure dependent resonance diameters $d_{s,r}(n^*) \pm 25\%$ of Table A2. This reduces the probability at water depths > 25 m, which requires bubble diameters > 6 mm at 2 kHz and > 1.5 mm at 8 kHz. The known appearance of relatively large, fast growing CO_2 bubbles, even after slow

and carefully opening of a pressurized champagne bottle, support our assumptions.

References

[1] M. Barmatz, P. Collas: Acoustical radiation potential on a sphere in plane, cylindrical and spherical standing wave fields. J. Acoust. Soc. Am. **77** (1985) 926–945.

[2] E. G. Lierke: Akustische Positionierung, ein umfassender Überblick über Prinzip und Anwendungen. Acustica **82** (1996) 220–237.

[3] E. G. Lierke: Deformation and displacement of liquid drops in an optimized acoustic standing wave levitator. Acta Acustica united with Acustica **88** (2002) 206–217.

[4] E. G. Lierke, L. Holitzner: Perspectives of an electrostatic / electrodynamic hybrid levitator for small fluid and solid samples. Measurement Science and Technology **19** (2008).

[5] E. H. Trinh, C. J. Hsu: Equilibrium shapes of acoustically levitated drops. J. Acoust. Soc. Am. **79** (1986) 1335–1338.

[6] C. P. Lee et al.: Static shape and instability of an acoustically levitated liquid drop. Phys. Fluids **A3** (1991) 2497–2515.

[7] E. G. Lierke et al.: Acoustic standing-wave-positioning of drops and bubbles in liquid filled resonance tubes. WCU (1995) 799–802.

[8] E. G. Lierke: tec5 AG, Oberursel: Equipment description and user instructions of ultrasonic levitators.

[9] E. G. Lierke, W. Littmann, D. Simon, T. Hemsel: To theory of piezoelectric compound transducers with practical hints to engineers (in German). http://ubdoc.unipaderbor.de /servlets/Document Serv let?id=12359, 2010.

[10] I. Veit: Flüssigkeitsschall. Kamprath-Reihe, Vogel-Verlag, 1979.

[11] E. G. Lierke et al.: Acoustic positioning for space processing of materials science samples in a mirror furnace. Proceedings of the IEEE ultrasonics symposium, Atlanta, GA, 1983, 1129–1139.

[12] E. G. Lierke: Nonlinearities in the open ultrasonic standing-wave-levitator at large acoustical Mach numbers. Proc. FEDSM'98, 1998 ASME Summer meeting, Washington, DC, 1998.

[13] E. G. Lierke: Controlled mass changes of drops in an acoustic standing-wave levitator (in German). Forschung im Ingenieurwesen – Engineering Research **62** (1996) 21–31.

[14] E. G. Lierke: Theoretical and experimental investigations to the ultrasonic cavitation in low viscous, gas solutions (in German). Dissertation RWTH Aachen, 1967.

[15] K. Yosioka, Y. Kawasima: Acoustic radiation pressure on a compressible sphere. Acustica **5** (1955) 176–178.

[16] K. Stamm: Investigation of the mechanism of the ultrasonic atomization at liquid interfaces with respect to technical applications (in German). Dissertation RWTH Aachen, 1964.

[17] C. A. Bjerknes: Hydrodynamische Fernkräfte. Ostwalds Klassiker d. Exakten Wissenschaft Nr. 195, Leipzig, 1915.

[18] E. G. Lierke: Technique and applications of ultrasonic atomizers – A look back on 35 years of research and development (in German). Chemie Ingenieur Technik. Kap. 2: Geyser atomizer **70** (1998) 815–826.

[19] Doku Deutschland. NDR film report 2007, Regie Volker Barth, reporter Antonelli Servidio: Warum stranden Wale, eine Detektivgeschichte (in German).

[20] Wikipedia: "middle-frequency" sonar.

[21] K. Bassner, C. Koch: Radiation pressure and interferometry as primary ultrasonic references. PTB-Mitteilung **117** (2007) Heft 1, p. 27ff.

[22] A. R. Kolaini, L. A. Crum: Bubble production by capillary-gravity waves. J. Acoust. Soc. Am. **95** (1994) 1913ff.

[23] Y. Mao, L. A. Crum, R. A. Roy: Nonlinear coupling between the surface and volume modes of an oscillating bubble. J. Acoust. Soc. Am. **98** (1995) 2764ff.